

González Ureña, A., Tremblay R, Rogers CA (2021) "Earthquake-resistant design of steel frames with intentionally eccentric braces", *Journal of Constructional Steel Research* 178: 106483.

Earthquake-Resistant Design of Steel Frames with Intentionally Eccentric Braces

Andrés González Ureña¹, Robert Tremblay², Colin A. Rogers³

¹ Ph.D. Candidate, Department of Civil Engineering and Applied Mechanics, McGill University, Montréal, QC. Email: andres.gonzalezurena@mail.mcgill.ca

² Professor, Department of Civil, Geological and Mining Engineering, Polytechnique Montréal, Montréal, QC. Email: robert.tremblay@polymtl.ca

³ Corresponding Author

Professor, Department of Civil Engineering and Applied Mechanics, McGill University, Montréal, QC. Email: colin.rogers@mcgill.ca

817 Sherbrooke Street West

Montréal, QC, Canada, H3A 0C3

Tel: 514 389 6449

ABSTRACT

Braces with Intentional Eccentricity (BIEs) have been proposed to overcome some of the shortcomings of Concentrically Braced Frames (CBFs), namely the implications of their inherently stiff nature, their limited post-yielding stiffness and the susceptibility of Hollow Structural Sections (HSSs) to premature local buckling and fracture, and the excessive overstrength that may result from the design codes limits on the local and global slenderness. However, the application of BIEs for use in buildings has not yet been attempted, nor has their implementation in a global design approach yet been addressed. In this paper, a procedure based on the Direct Displacement Based Design (DDBD) method is employed in the seismic design of Frames with Intentionally Eccentric Braces (FIEBs). Buildings of 4, 8 and 12 storeys are designed as FIEBs with HSS brace members, with target drift ratios of 1.5 % and 2.5 %, and as Special CBFs for comparison purposes. The performance of the resulting buildings is assessed through Non-Linear Response-History Analysis. The results show that the employed design procedure is well suited to FIEBs, that their seismic performance is satisfactory and complies with the proposed performance objectives, and that they can constitute an economically advantageous alternative to conventional CBFs.

Keywords: steel braced frames; eccentric braces; earthquake-resistant design; displacement-based design

1. INTRODUCTION

Concentrically Braced Frames (CBFs) with Hollow Structural Sections (HSSs) as the brace members are widely used as the seismic-force-resisting system (SFERS) of low- and mid-rise buildings. Despite their popularity, these structures present significant drawbacks that hinder their convenience. Firstly, the ductility and the energy dissipation capacity of the braced frame is limited by the susceptibility of HSS braces to low cycle fatigue induced fracture at the plastic hinge region [1,2]. Secondly, due to their invariably stiff nature, CBFs are constrained to low fundamental periods of vibration and, thus, to high acceleration and force demands, which, in combination with the overstrength that originates from the compression resistance governing the sizing of the brace members, result in high design forces for the capacity protected components of the structure and its foundations, weighing significantly on the total cost of construction. Additionally, Conventional Concentric Braces (CCBs) possess nearly no post-yielding stiffness, potentially resulting in large deformation demands and stability issues. Furthermore, although the design codes prescribe limits to the local and global slenderness of the bracing members in CBFs aiming to ensure that they provide an adequate response and sufficient ductility, the need to comply with these often results in unintentional excessive overstrength in particular storeys, favouring the concentration of drift demands in storeys with a lower capacity to demand ratio [3]. The propensity of CBFs to develop a soft-storey seismic response is mitigated by the modest force modification factors and stringent building height limits specified in the codes, further hindering their cost-effectiveness and range of application in seismically active regions.

To overcome these shortcomings of CCBs, Skalomenos et al. [4] proposed the use of Braces with Intentional Eccentricity (BIEs) as an alternative lateral load carrying system. A BIE is, straightforwardly, an otherwise conventional brace with its longitudinal axis offset with respect to the working points (i.e. the frame diagonal). As, due to this eccentricity, they are subjected to

bending moment and axial force simultaneously under seismic action, BIEs are naturally more flexible than CCBs and are characterised by a pseudo-trilinear force-displacement behaviour in tension, with an early initiation of inelastic response and significant post-yielding stiffness, and a smooth flexural response in compression devoid of sharp peaks and loss of stiffness due to sudden buckling. Moreover, their pre- and post-yielding stiffness can be controlled by varying the prescribed eccentricity, enabling a better control over the dynamic response of the structure. These characteristics of BIEs presumably auspice an earlier and better distributed engagement of dissipative action. In addition to this, the onset of local buckling at the mid-length, which precedes fracture, is delayed in terms of axial displacements because the strain demand is more evenly distributed along the brace length. In their research, Skalomenos et al. performed cyclic load tests on five half-scale BIE specimens with two eccentricity values and one CCB, all made from the same circular HSS, and obtained results consistent with the behaviour described above. However, their published works did not address the application of these braces in buildings nor did they speak to the implementation of BIEs in a global design approach. These steps are necessary to determine whether BIEs would indeed produce SFRSs with advantages, in terms of cost or structural performance, over conventional CBFs.

In this paper, an exploratory investigation on the seismic design and performance of Frames with Intentionally Eccentric Braces (FIEBs) made of square HSSs is presented. Given the particular force-deformation behaviour of BIEs, which, as is herein described, sets them apart from conventional dissipating elements, an alternative design approach addressing explicitly the characteristics of the BIEs, namely one based on the Direct Displacement-Based Design procedure, was developed. Prototype buildings based on a common plan configuration and with number of storeys of 4, 8 and 12, were designed using the proposed design procedure for two target maximum drift ratios: 2.5 % and 1.5 %. To consider a relatively high seismic hazard, the buildings were supposed located in Los Angeles, CA, on a class C site, resulting in seismic design category D, according to ASCE/SEI 7-16 [5]. The braces were designed to bend in the plane of the frame using

a knife-plate to gusset-plate connection. The eccentricity was achieved by means of side-plated assemblies linking the bracing members to their connections to the frame beam-to-column joints, designed following constructive and cost-effectiveness criteria. To allow for the comparison of costs and structural performance, conventional Special CBFs were also designed for the same conditions. The performance of all resulting frames under seismic action was assessed numerically through Non-Linear Response-History Analyses (NLRHA) on fiber-based models in OpenSees [6].

2. CHARACTERIZATION OF BIEs

2.1. Components of BIEs

The essential components of a nonspecific BIE are presented schematically in Fig.1. The eccentricity, e , is defined as the parallel offset between the axis of the bracing member and the line connecting the frame's working points, which would normally coincide with the frame diagonal. The eccentricity is introduced by assemblies that transfer rigidly the axial loads between the working points and the bracing member, hereon designated as *eccentering* assemblies. Beyond their length, L_{ea} , the specific design of the *eccentering* assemblies does not have a significant effect on the response of the BIE provided that they can be assumed to behave as rigid bodies linking the bracing member to its connection to the rest of the structure. Examples of *eccentering* assemblies are those tested by Skalomenos et al. and the ones considered in this research, which are described further below. The total, or hinge to hinge, length of the BIE is L .

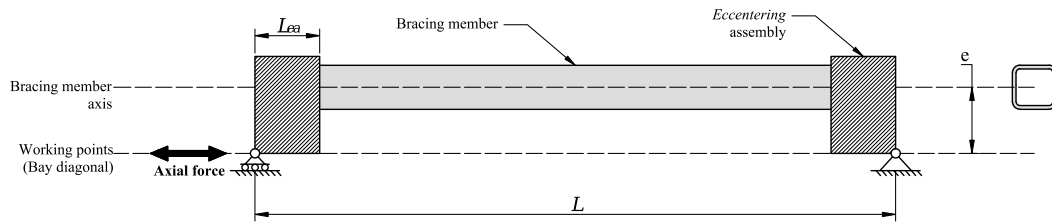


Fig. 1. Schematic drawing of a nonspecific BIE and its components

2.2. Modelling of BIE response

In this research, the OpenSees platform is the main resource used to model BIEs and to study their response and the effects of the different variables involved. OpenSees allows for the construction

of fiber-based finite element frame objects incorporating the specified material stress-strain curve and force-deformation hysteretic parameters at the fiber level and, as such, allows for the explicit representation of distributed plasticity. The software is also capable of handling geometric nonlinearity and is therefore well suited to reproduce the global response of steel frames with elements under flexural compression, including buckling of braces. OpenSees has been used extensively in research on steel frame structures and its suitability for these purposes has been demonstrated in many publications [7,8]. Since the published data on the numerical modelling of BIEs is scarce, the authors verified the applicability of OpenSees for BIEs by programming models of the tests described in Skalomenos et al. and verifying that the numerical results were in reasonable agreement with the published test results.

Fiber-based finite element models, however, possess the limitation of being unable to capture localized phenomena such as local buckling, which is of great relevance as an indicator of the imminent failure of HSS brace members. Therefore, the OpenSees analyses are complemented in this research with shell-based finite element models in the commercial software Abaqus [9] when there is need to explicitly capture the onset of local buckling, as is explained in section 2.7. The suitability of Abaqus for this purpose has also been demonstrated in the literature [10].

2.3. Monotonic Force-Deformation Behaviour of BIEs

The kinematic response of BIEs, which was described in Skalomenos et al., and is here anew summarized, relies on the assumption that the connections at the ends of the *eccentering* assemblies behave as pins. In practice, this can be reasonably approximated by employing ductile connections detailed to yield in flexure at low levels of axial load such as those commonly used in CBFs. The idealised general behaviour of BIEs under tensile (a) and compressive (b) monotonic load, compared to that of CCBs, is presented in Fig.2. Due to the eccentric loading, bending moments develop at its ends with initial magnitude equal to the product of the force and the prescribed eccentricity. Under tensile load, the BIE bends toward the working point axis as it elongates and, since the moment arm across the brace length decreases as the loading progresses, the effective

stiffness increases with the axial deformation until the outermost fiber in tension attains the yielding stress, F_y . The corresponding point on the curve, $T_y - \Delta_y$, marks a discontinuity on the force-deformation response, and is designated as the “first yield” point. As loading is continued beyond this stage, the plasticity extends through the cross-section and the BIE responds with a lower stiffness that, however, increases as the effective eccentricity keeps decreasing. The maximum tensile force developed by the BIE, T_u , is attained when the effective eccentricity where the bracing member meets the *eccentering* assembly reaches zero, thus allowing the full cross-section to yield in tension. Nearing this stage, depending on the magnitudes of e and L_{ea} , plastic hinges may develop where the brace ends meet the *eccentering* assemblies because bending of the HSS compensates the rotation of the *eccentering* assemblies in order to maintain the parallelism between the bracing member’s axis and the frame diagonal. The maximum rotation demand on the HSS at that location, θ_{t_u} , can be estimated as $\tan^{-1}(e/L_{ea})$. As shown in Fig. 2 (a), the force-deformation backbone curve of BIEs in tension can be approximated with a tri-linear model, as proposed in Skalomenos et al. An initial, or elastic, portion with stiffness K_i extends up to the “first yield” point, T_y , followed by a post-“first yield” portion, with secondary stiffness K_s , limited by the ultimate yield point, T_u . This is trailed by a final segment, comprising the fully yielded section, that extends until the brace eventually fractures.

When compressive load is applied, the BIE bends away from the working point axis and the increment of the brace deflection entails a progressive reduction of the stiffness, as the effective eccentricity at the brace mid-length increases. As proposed by Skalomenos et al., the maximum force developed in compression, C' , can be approximated by the load corresponding to the elastic limit state of a column subjected to eccentric axial load, using Eq. (1), where P_{cr} is Euler’s buckling load, A is the cross-section’s area and S is the section modulus.

$$C' = \frac{F_y A}{1 + \frac{eA}{S \cos\left(\frac{\pi}{2} \sqrt{\frac{C'}{P_{cr}}}\right)}} \quad (1)$$

In contrast with CCBs, in BIEs the maximum force in compression does not manifest as a sharp peak in the force-deformation curve. Instead, their response transitions smoothly from elastic to inelastic post-buckling behaviour. As such, the backbone curve of BIE response in compression can be idealised as elastic-perfectly plastic, with initial stiffness K_i and maximum force C' as shown in Fig. 2 (b). As the deformation progresses, a plastic hinge develops at the brace-mid-length where the strain demand concentrates. As it will be explained, the set composed by T_y , T_u , C' , K_i , and K_s comprises the relevant parameters used for design, which depend on the length, cross section and eccentricity of the BIE.

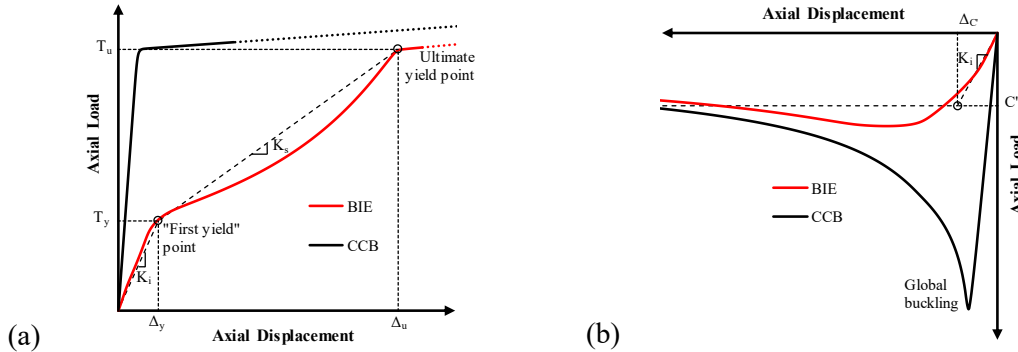


Fig. 2. Compared BIE and CCB idealised monotonic force-deformation behaviour: tension (a) and compression (b) (not to scale)

The effects of the eccentricity magnitude on the BIE's monotonic response can be observed in Fig. 3, which, as an example, presents the results of analyses carried out in OpenSees on models of BIEs of an ASTM A1085 HSS 178×178×16 for different levels of eccentricity under monotonic tensile (a) and compressive (b) loading. The length of the BIE for these models was 5408 mm, including *eccentering* assemblies modelled as 360 mm long rigid links. The end connections were modelled as 38.1 mm thick plates with a width of 360 mm and a clearance of 77 mm to allow for unrestrained plastic rotation and to resist the force associated with the probable brace resistance in tension. The design is consistent with that of a BIE intended for a 6 m wide by 4 m tall braced bay considering

a knife plate to gusset plate end connection producing in-plane bending of the BIEs, as is discussed below. A nominal yield stress of 345 MPa was considered both for the plates and the HSS for these analyses. Referring to the idealized models of BIE response described above, the relevant values for design, i.e. T_y , T_u , C' , K_i , and K_s , can be obtained from such analyses. Table 1 presents this set of parameters, as obtained from the curves shown in Fig. 3. In general, for a given section BIE, T_y , C' , K_i , and K_s will decrease as a function of the eccentricity, resulting in an increase of the deformations associated with “first yield” and ultimate yield. The ultimate yield force, T_u , does not depend on the eccentricity, as it is a function of the section’s gross area and material yield stress.

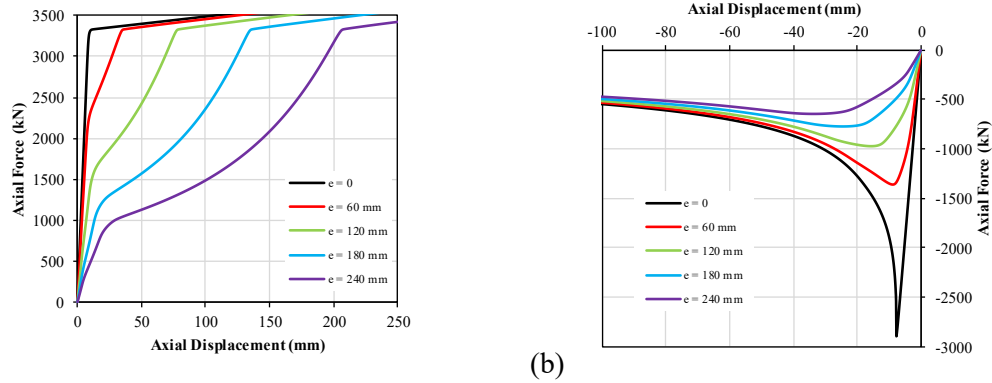


Fig. 3. Influence of eccentricity on the force-displacement response of HSS 178×178×16 BIEs with $L=5408$ mm and $L_{ea}=360$ mm: tension (a) and compression (b)

Table 1. Example of selected relevant design values as a function of eccentricity for HSS 178×178×16 BIEs with $L=5408$ mm and $L_{ea}=360$ mm

Eccentricity, e , (mm)	“First yield” force, T_y , (kN)	Ultimate yield force, T_u , (kN)	Compressive resistance, C' , (kN)	Initial stiffness, K_i , (kN/mm)	Secondary stiffness, K_s , (kN/mm)
0	-	3325.8	1788.3	356.5	-
60	2088.1	3325.8	1032.7	271.2	44.8
120	1471.2	3325.8	716.1	136.2	27.6
180	1135.8	3325.8	554.9	69.7	18.4
240	926.2	3325.8	454.9	39.4	13.1

Taking the horizontal components of the axial forces obtained for the analyses shown in Fig. 3 and summing them, one obtains the storey shear force that two contiguous braced frames with bracing members such as described above acting in opposite directions would produce when subjected to horizontal displacement at the top, as presented in Fig. 4. Note that in contrast with the CCBs (i.e. $e = 0$), the storey shear response of the BIEs with significant eccentricities working in pairs increases continuously with the displacement; there is no peak corresponding to buckling of the compression brace and subsequent drop in storey shear capacity. As is discussed below, the

eccentricity to bracing member section depth ratios (e/H) that commonly result from the use of the design procedure herein described are larger than 0.66, and therefore the shear – deformation stiffness of the BIE pairs is continuously positive.

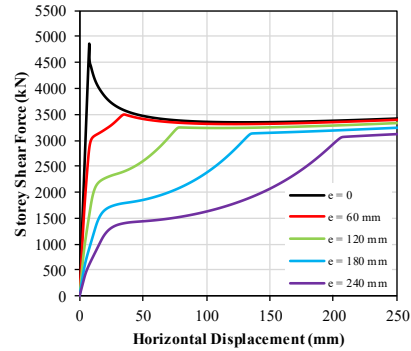


Fig. 4. Influence of eccentricity on the storey shear vs. top displacement response for two contiguous 6 m by 4 m bays with HSS 178×178×16 BIEs acting in opposite directions.

2.4. Influence of the *eccentering* assemblies length

The length of the *eccentering* assemblies, L_{ea} , plays a significant role on the force-deformation response of BIEs in tension, and should thus be incorporated explicitly in any BIE model. Firstly, the bending moments that develop on the bracing members' ends and how they evolve as the brace elongates and bends toward the working point axis depend on the dimensions of the *eccentering* assemblies. For a given eccentricity, an increase of L_{ea} implies a reduction of the maximum rotation demand, $\theta_{t,u}$, thus decreasing the displacement required to annul the eccentricity and reach the ultimate yield point. Also, supposing that the total length, L , remains unchanged, an increase of L_{ea} results in a reduction of the length of the deformable bracing member, and therefore in an increase of the axial stiffness of the BIE. An example of this can be observed in Fig. 5 (a), which presents the monotonic force-deformation curves in tension for a set of BIE models with varying L_{ea} . The values of K_i and K_s , and hence the “first yield” and ultimate yield deformations, depend on the length of the *eccentering* assemblies. The response in compression, however, is not significantly affected by the magnitude of L_{ea} , as Fig. 5 (b) shows, presumably because the stiffness of the

compression response mainly depends on the rotational rigidity of the mid-length region and the end connections.

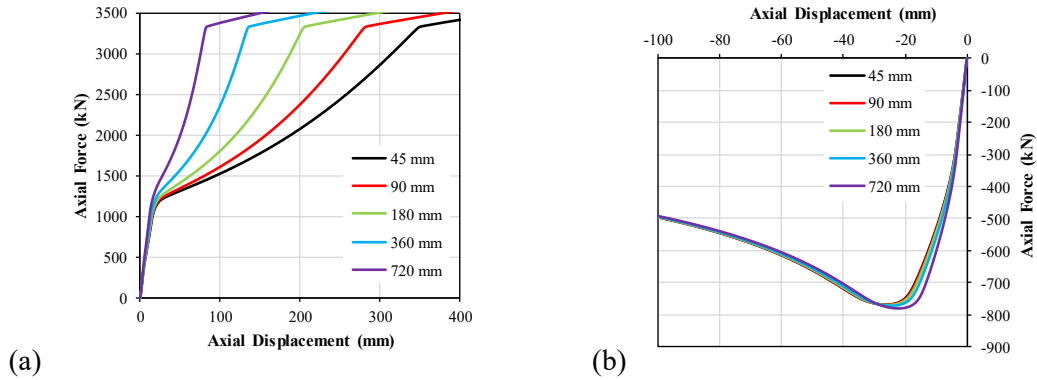


Fig. 5. Influence of L_{ea} on the force-displacement response of HSS 178x178x16 BIEs with $L=5408$ mm and $e=180$ mm: tension (a) and compression (b)

2.5. Influence of residual stresses and in-section variation of F_y of BIEs

Due to their fabrication process, which involves rolling and cold working, HSSs contain residual stresses and present a variation of the yield stress, F_y , across their cross section. Koval [11] presents a thorough review of the available research on the topic and proposes a model of the distribution of the residual stresses and yield stress gradient over the thickness and the perimeter of rectangular HSSs, applicable to fiber elements models in OpenSees. A comparison of the monotonic force-deformation response of an OpenSees BIE model that neglects the residual stresses and yield stress gradient against one that includes these effects using Koval’s model is presented in Fig. 6. In the latter, only the variation of the residual stresses across the thickness was considered, as it was shown by Koval that the variation across the perimeter exerts no significant influence on an HSS’s force-deformation response. Considering the nominal value for F_y of 345 MPa, the net yield stress on the model with the effects was uniformly scaled so that both models had an equal ultimate tensile strength. As can be seen, the effects of the residual stresses and yield stress gradient do not modify considerably the response in monotonic tension, producing only slight changes to the shape of the curve and to the displacements corresponding to “first yield” and ultimate yield. In compression, the inclusion of the effects results in an even smoother transition from the elastic to the post-buckling regimes.

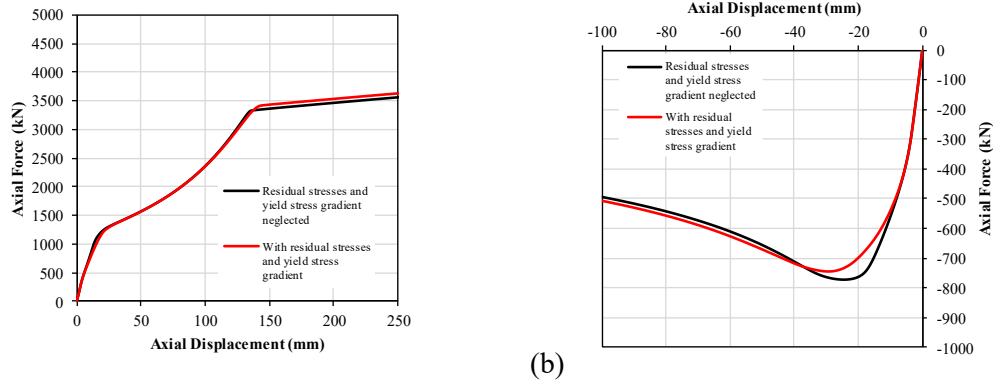


Fig. 6. Influence of yield stress gradient and residual stresses on the force-displacement response of HSS 178×178×16 BIEs with $L=5408$ mm and $e=180$ mm: tension (a) and compression (b)

2.6. Response of BIEs to Cyclic Loading

The axial force vs. lateral drift hysteretic plots of an ASTM A1085 HSS 178×178×16 BIE with an eccentricity of 180 mm, and a CCB of the same section, are presented in Fig. 7 (a). The resulting storey shear vs. lateral drift plots that would result from pairs of such braces acting in opposing directions in adjacent bays are shown in Fig. 7 (b). The data were obtained from OpenSees analyses where the brace dimensions and components were, again, defined assuming a 6 m wide by 4 m tall braced bay. A loading protocol with symmetrical cycles of increasing equivalent storey drift amplitude of 0.1, 0.25, 0.75, 1.0, 1.5, 2 and 3 % was followed. In Fig. 7 (a), it can be noted how, in contrast with the CCB, the BIE exhibits a significant secondary (post “first yield”) stiffness in tension with the maximum load increasing at each cycle, while in compression the maximum load stabilizes at the post-buckling force level. These properties are conserved when two braces act jointly, as seen in Fig. 7 (b).

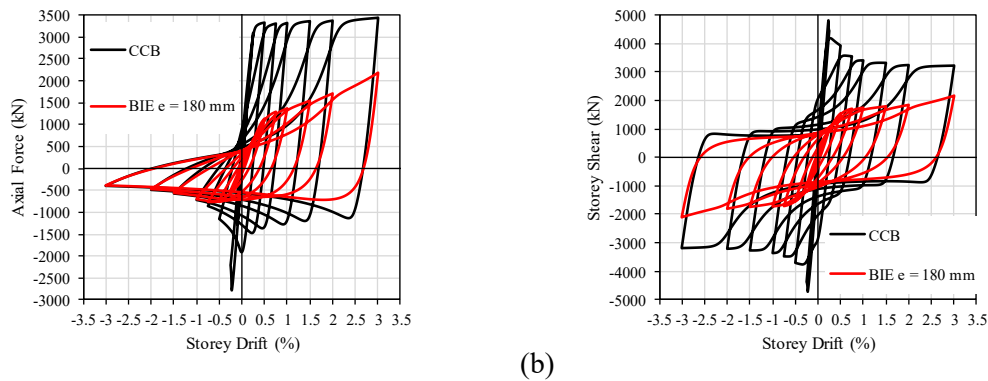


Fig. 7. Single brace axial force vs. lateral drift (a) and storey shear vs. lateral drift (b) for HSS 178×178×16 CCBs and BIEs with $e = 180$ mm under cyclic load.

2.7. Fracture Life of BIEs

As for conventional braces, low-cycle fatigue fracture, triggered by local buckling, presumably governs the failure mode of HSS BIEs. However, the physical tests by Skalomenos et al. showed that the introduction of eccentricity delays the onset of local buckling at the brace mid-length in terms of axial displacement or equivalent inter-storey drift ratio. This is explained by the strain demands being more evenly distributed along the brace length due to the presence of bending from the onset of loading. To generalize these findings to BIEs made with square HSSs commonly used in North America, i.e. ASTM A1085 HSSs, the authors performed a parametric study based on 243 individual finite element BIE models in Abaqus based on standard commercially available sections and dimensioned assuming the use of the braces in a 6 m by 4 m braced bay. The considered variables were the global (L/r) and local (b/t) slenderness ratios and the eccentricity ratio, defined as the specified eccentricity divided by the section height, $e_0 = \frac{e}{H}$. Given the lack of available data necessary to adequately calibrate a material damage model to capture low-cycle fatigue fracture in BIEs, the onset of local buckling at the brace mid-length was regarded as an indicator of imminent failure. It has been shown in previous research on HSS braces [1, 2, 12] that once local buckling occurs, the brace will likely fracture in the subsequent tension excursion. The BIE models in the study were subjected to reversed cyclic loading with increasing displacement amplitude; the drift ratio of the cycle with maximum amplitude that the BIE could sustain before developing local buckling was reported as the maximum allowable drift ratio, θ_{md} . The maximum drift ratio amplitude in the load protocol was 5 %; this value was reported for the models that did not show local buckling during the analyses. As expected, the results illustrate that the fracture life of BIEs increases with the eccentricity, the global slenderness and the stockiness of the section. A multiple regression analysis was then applied to obtain an expression to estimate θ_{md} as a function of e_0 and a combined slenderness ratio: $\lambda_0 = \frac{Lt}{rb}$, given in Eq. (2). The data point scatter and the surface corresponding to the obtained function are shown in Fig. 8. It must be noted, however, that the

appropriateness of the proposed equation is yet to be validated by contrasting the drift ratios at the onset of local buckling it predicts, against actual results from physical testing of BIE specimens.

$$\theta_{md} = -0.4312 + 0.1943\lambda_0 + 0.6704e_0 - 0.001319\lambda_0^2 - 0.01833\lambda_0e_0 + 0.241e_0^2 \quad (2)$$

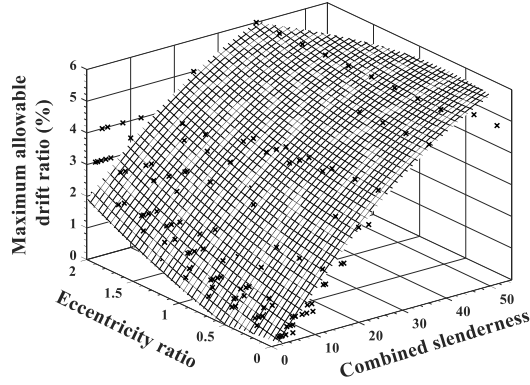


Fig. 8. Maximum allowable drift ratio vs. eccentricity ratio and combined slenderness

2.8. Energy Dissipation Capacity of BIEs

In comparison with CCBs, a larger amount of energy is required to reach the tensile yield strength of BIEs. This is due to the additional energy required to straighten the bracing member and annul the eccentricity. In Fig. 9, the total energy required to attain T_u , disaggregated into its axial and flexural components, is presented for an ASTM A1085 HSS 152×152×13 BIE with different levels of eccentricity. To construct this plot, first the energy required to attain T_u for a perfectly straight brace was obtained from an analysis under monotonic load in OpenSees. This energy is thus associated with the axial elongation of the brace (blue part of the bars in Fig. 9). Then, the analysis was replicated for increasing e/H ratios, and the difference in the total energy with respect to the concentric model is assumed to be associated with bending (red part of the bars). As expected, the flexural energy increases with the eccentricity, whereas the axial energy does not vary. However, as the eccentricity is increased, the displacement required to reach T_u increases accordingly. As such, although it would be impractical to fully benefit from the maximum theoretical energy dissipation capacity of BIEs in design, as the displacement involved could be excessive. However, one could still benefit from part of the additional energy dissipation by performing a design oriented

toward the BIEs attaining a predetermined and practical, drift or displacement target under seismic action. The energy dissipation capacity at the target displacement could then be exploited in design through an equivalent damping ratio.

The equivalent damping ratio, ξ_{eq} , quantifies the net damping capacity of a dissipative system under cyclic loading for a given loading cycle accounting for all the energy-dissipating mechanisms involved [13]. ξ_{eq} can be obtained from Eq. (3), where E_d is the area enclosed by the force-deformation curve for the cycle of interest, and F_m and Δ_m are respectively the maximum force in the cycle and the displacement amplitude.

$$\xi_{eq} = \frac{E_d}{2\pi F_m \Delta_m} \quad (3)$$

Skalomenos et al. presented the equivalent damping ratios, ξ_{eq} , obtained for their test specimens at each drift level. It was shown that although the maximum values of ξ_{eq} were not significantly affected by the eccentricity, the drift ratio at which they occurred varied notably as the yield displacement changed with the eccentricity. Preliminary data collected from numerical analyses performed by the researchers on BIEs have shown that, indeed, there is no clear correlation between the eccentricity and the net energy dissipation capacity. Further, the eccentricity has no notable effect on the equivalent damping ratio as a function of the ductility demand. The ductility demand is defined as the ratio between the cycle amplitude and the drift corresponding to the “first yield” point of the BIE. An example of this behaviour is presented in Fig. 10 for ASTM A1085 HSS 152×152×13 BIEs, in which it can be observed that for eccentricity ratios equal to 1.0 or larger, the maximum value for ξ_{eq} and the associated ductility demand are practically constant.

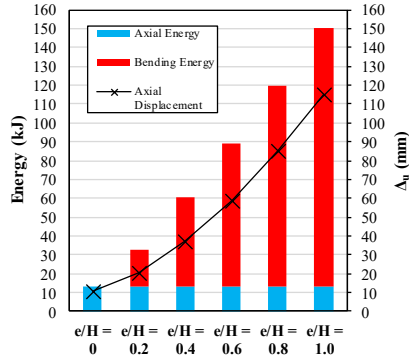


Fig. 9. Energy input and axial displacement required to reach T_u under monotonic loading for HSS $152 \times 152 \times 13$ BIEs with $L=5408$ mm and $L_{ea}=305$ mm

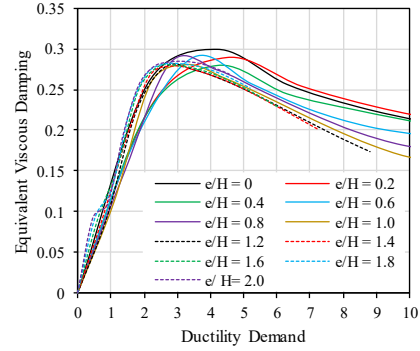


Fig. 10. ξ_{eq} vs. ductility demand for HSS $152 \times 152 \times 13$ BIEs with $L=5408$ mm and $L_{ea}=305$ mm

2.9. Sensitivity to Member Out-of-Straightness

While in CCBs the member out-of-straightness plays an important role on the brace buckling strength, in BIEs, given that their responses in compression and in tension encompass an inherent flexural component, the effect of the member imperfection is overshadowed by that of the eccentricity. Depending on whether the out-of-straightness increases (positive out-of-straightness) or decreases (negative out-of-straightness) the effective eccentricity, it may entail an increment or decrement in the BIE strength and stiffness. As positive out-of-straightness increases, the effective eccentricity at mid-length, the values of K_i , K_s , C' , and T_y decrease accordingly. Conversely, with negative out-of-straightness those values increase. Numerical analyses carried out by the authors to study the influence of member out-of-straightness on the monotonic and cyclic response of BIEs indicate that the effects of out-of-straightness smaller than $\pm L/1000$, the fabrication tolerance in North American codes [14, 15], are negligible. Figure 11 presents the change of the compressive strength of BIEs as a function of the out-of-straightness with respect to the compressive strength of a perfectly straight BIE, C'_0 , as obtained from OpenSees models of BIEs with different global slenderness and eccentricities. The results show that the influence of the out-of-straightness is greater for smaller eccentricities and larger slenderness; however, for out-of-straightness within the $\pm L/1000$ tolerance, which corresponds with the region highlighted in gray in Fig. 11, the differences are within $\pm 5\%$.

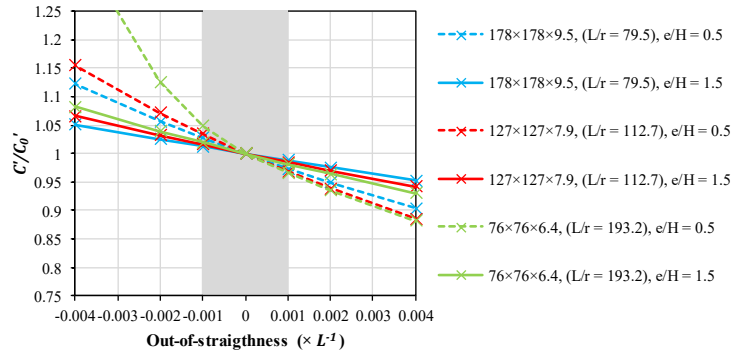


Fig. 11. Change of the compressive strength of BIEs as a function of the out-of-straightness, with respect to the compressive strength of a perfectly straight BIE

3. DESIGN PROCEDURE FOR FIEBs

As shown in the previous section, BIEs present a particular force-deformation behaviour that makes them stand out from traditional dissipative elements used in SFRSs, such as CCBs, moment frame connections or eccentrically braced frame links, among others. The monotonic response of common SFRSs can be reasonably approximated by elastic-perfectly plastic models; they respond elastically until they reach their yield resistance, at a relatively low displacement or rotation, and then, if the loading is continued, they deform plastically with the force or moment remaining at an essentially constant level until fracture. Considering this, traditional dissipative elements are well suited for the force-based design methods that most modern design codes wield; they can be dimensioned by equating their yield strength to the seismic demand resulting from an elastic analysis, in which the force level is reduced to account for ductile response and overstrength. In the case of BIEs, however, the maximum capacity in tension is attained at variable deformation levels that depend on the eccentricity and that might even be larger than the maximum inter-storey drift ratios allowed by the design codes, e.g. 2.0 % in ASCE/SEI 7-16 for buildings over 4 storeys high and 2.5 % for buildings with 4 or fewer storeys. Furthermore, BIEs' secondary stiffness is significant and also varies with the eccentricity, the section properties and the brace geometry, making both the elastic-perfectly plastic idealisation and the use of a ductility related seismic force reduction factor unfitting.

Given these considerations, the use of a displacement-based design method, allowing for the explicit consideration of the force the BIEs develop as a function of the axial displacement, appears as a rational course of action. Specifically, an adaptation of the Direct Displacement-Based Design method (DDBD) [16], is here employed. In past research, the appropriateness of the DDBD approach for the seismic design of multiple types of structures, including CBFs [17, 18], has been demonstrated; the results presented in this paper can be considered a verification of its applicability to FIEBs. In the following sections, a description is given of the steps of the adapted design procedure as used in this research. For general information on the DDBD method, refer to [16].

3.1. Selection of design target storey drift and displacement vector and calculation of associated equivalent mass and equivalent displacement

In DDBD, the target displacement vector generally corresponds to the inelastic first mode shape of the structure and, as such, is specific for the structural system and the height of the building. It is important to note this target displacement vector is a design assumption that does not necessarily reflect the distribution of anticipated maximum storey displacements, as it does not account for the effects of higher modes or the reversing nature of earthquake demands. Expressions are available to approximate the inelastic first mode shape of various traditional structural systems, but in the case of FIEBs, none are yet available as the research on the new structural system is incipient. Moreover, the formal calibration of such expressions requires a considerable amount of data and work which, in the authors' opinion, will be justified at a later stage once the potential of the new system will have been established.

In this research, the inelastic first mode shape proposed by Priestley et al. [16] for moment frames, given in Eq. (4) is used. Although expressions developed for CBFs exist, such as the one presented by Al-Mashaykhi et al. [19], and arguably that system bears more similarities to the proposed system than moment frames, analyses by the authors have shown that the inelastic first mode shape of FIEBs is in fact closer to the shape obtained with Eq. (4) than to that obtained with the expressions for CBFs. An example of this is presented in Fig. 12. A proposed explanation for this

observation is that, given that BIEs are naturally less stiff than CCBs, the displacement profile of FIEBs is closer to that of an ideal shear building, in contrast with CBFs where the contribution to the deformed shape of the axial deformations of the columns is more significant. In Eq. (4), n is the number of storeys, H_i and H_n are the elevations of the i^{th} and top storeys and δ_i is the normalised lateral displacement of the i^{th} storey.

$$\begin{aligned} n \leq 4: \quad \delta_i &= \frac{H_i}{H_n} \\ n > 4: \quad \delta_i &= \frac{4H_i}{3H_n} \left(1 - \frac{H_i}{4H_n}\right) \end{aligned} \quad (4)$$

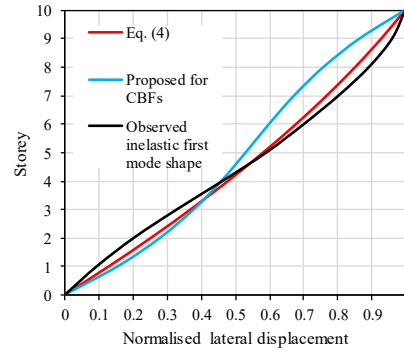


Fig. 12. Observed inelastic first mode shape of a 10 storey FIEB, compared with predicted inelastic first mode shapes for moment frames and CBFs

The normalised displacement vector obtained with Eq. (4) is then scaled to produce the selected lateral design drift of the critical storey, which is the first storey for buildings 5 storeys and taller, to obtain the storey design displacements, d_i , which, along with the storey masses, m_i , are used in the calculation of the displacement (Eq. (5)) and mass (Eq. (6)) of the equivalent Single Degree of Freedom System (SDOF) at the design level.

$$\Delta_{eq} = \frac{\sum d_i^2 m_i}{\sum d_i m_i} \quad (5)$$

$$M_{eq} = \frac{\sum d_i m_i}{\Delta_{eq}} \quad (6)$$

3.2. Determination of equivalent damping ratio and target period

The target period, T_{eq} , is obtained from the damped displacement design spectrum by reading the ordinate corresponding to Δ_{eq} . To do so, however, the equivalent viscous damping ratio, ξ_{eq} , used to reduce the displacement spectrum must first be defined. In the same manner as for the displacement vector, no models exist yet for the estimation of the equivalent viscous damping of FIEBs in the context of DDBD. The formal development of such models remains for the moment out of the scope of this exploratory investigation. In lieu of that, the models proposed by Wijesundara et al. [20] for the equivalent damping ratio of CCBs as a function of the member's non dimensional slenderness, λ , and the ductility demand, μ , given by Eq. (7) are used. This approach is considered acceptable since, as is explained in the previous section, for BIEs, ξ_{eq} as a function of μ is not sensibly affected by the variation of the eccentricity level and because, as is shown below, the results obtained using this approach are satisfactory.

$$\begin{aligned} \mu \leq 2: \quad \xi_{eq} &= 0.03 + \left(0.23 - \frac{\lambda}{15}\right)(\mu - 1) \\ \mu > 2: \quad \xi_{eq} &= 0.03 + \left(0.23 - \frac{\lambda}{15}\right) \end{aligned} \quad (7)$$

$$\lambda = \frac{L}{r} \sqrt{\frac{F_y}{\pi^2 E}}$$

Eq. (7) gives ξ_{eq} for a pair of identical braces acting together in opposite direction. Thus, assuming that only one type of BIE is used per storey, the average value from all storeys is used to obtain the design ξ_{eq} of the FIEB, which is then used to reduce the base displacement spectrum through the damping correction factor, R_ξ . In this research, the damping correction factor recommended by Eurocode 8 [21], given by Eq. (8) is used. The base design displacement spectrum, S_d , is obtained by applying Eq. (9) to the 5 % damping elastic design acceleration spectrum, S_a .

$$R_\xi = \sqrt{\frac{0.1}{0.05 + \xi_{eq}}} \quad (8)$$

$$S_d = S_a \frac{T^2}{4\pi^2} \quad (9)$$

3.3. Calculation of target “primary” target secant stiffness, associated base shear and equivalent static force vector

Having obtained T_{eq} , the target “primary” secant stiffness, K_{eq} , can be calculated with Eq. (10). The authors refer to this stiffness as “primary” since it is directly associated with the target spectral displacement of the equivalent SDOF system. Additional “auxiliary” stiffness might also need to be provided to the FIEB to comply with stability and regularity criteria, as explained below. The primary base shear, V_{eq} , is obtained by multiplying K_{eq} by Δ_{eq} (Eq. (11)), and subsequently can be distributed as the corresponding storey lateral forces, F_i . In this research, the distribution of storey forces is performed as per Clause 12.8.3 of ASCE/SEI 7-16 (Eqs. (12) and (13)); however, instead of the initial period, T_{eq} is used to compute the exponent k in acknowledgment of the structure’s anticipated condition at the design level. In Eq. (13), for structures with $T_{eq} < 0.5$ s, $k = 1$; for structures with $T_{eq} > 2.5$ s, $k = 2$; and for structures with T_{eq} between these two values, k is interpolated linearly.

$$K_{eq} = 4\pi^2 \frac{M_{eq}}{T_{eq}^2} \quad (10)$$

$$V_{eq} = K_{eq} \Delta_{eq} \quad (11)$$

$$F_{eq,i} = C_{vi} V_{eq} \quad (12)$$

$$C_{vi} = \frac{W_i h_i^k}{\sum_{i=1}^n W_i h_i^k} \quad (13)$$

3.4. Selection of BIEs for each storey, providing capacity equal to the *design shear* at the design displacement level and complying with regularity and stability criteria

At each storey, the BIEs, in terms of a section-eccentricity pair (e.g. HSS 178×178×16 – e = 230 mm) are selected such that the storey shear capacity they provide at the target storey displacement, d_i , is equal to the *design shear*. The storey *design shear*, $v_{d,i}$, given by Eq. (14), is defined as the

sum of the equivalent primary storey shear, $v_{eq,i}$ (i.e. the cumulated effects of the forces $F_{eq,i}$ above storey i obtained from step 3), and the notional loads, $v_{n,i}$, amplified by a factor accounting for the P- Δ effects which, given that FIEBs are relatively flexible structures, if not addressed in the design might induce a reduction of the effective stiffness of the structure as it evolves toward the design displacement. In this paper, the magnitude of the notional loads applied corresponds to 0.002 times the factored gravitational loads, $C_{f,i}$, as per clause C2.J.2b of ANSI/AISC 360-16 [14]. The amplification factor used to account for the P- Δ effects at the design level, $U_{2,i}$, is based on that of CSA S16-14 Clause 27.1.8.2 [15], given by Eq. (15), where v_i^* is the storey shear capacity of the chosen section-eccentricity pair at the design displacement level. This amplification factor is preferred over that given by clause 12.8.7 of ASCE/SEI 7 as it compensates the loss of storey shear resistance due to P- Δ effects at the expected displacement.

$$v_{d,i} = U_{2,i}(v_{eq,i} + v_{n,i}) \quad (14)$$

$$U_{2,i} = 1 + \left(\frac{C_{f,i}d_i}{v_i^*h_i} \right) \quad (15)$$

The selection of the BIE section-pairs can rely on simplified models of the monotonic behaviour of the BIEs in tension and compression, such as those described in Section 2.3 (cf. Table 1). These can be obtained from numerical analyses under monotonic load performed on fiber-element models based on the design properties of the material (i.e. F_y), and considering the actual dimensions the BIE will have in the braced bent, in particular its total length, L , and the length of the *eccentering* assemblies, L_{eq} . To ensure that the resulting FIEB indeed attains safely the intended displacement levels, the fracture life of the selected section-eccentricity pairs needs to be considered. This can be performed by verifying that the allowable drift, calculated with Eq. (2), is at least 50 % higher than the design drift to include a safety margin.

In addition to providing sufficient capacity to satisfy the *design shear*, the BIEs shall also comply in each storey with minimum stability and regularity criteria to favour an adequate response of the

structure. To prevent geometric instability, the ratio of effective lateral stiffness to counterbalancing geometric stiffness at the design displacement level should be at least 1.5, as through several preliminary evaluations, the authors have found that satisfying this limit reduces the probability of collapse due to geometric instability. Similarly, it was found that, to avoid soft-storey mechanisms and concentrations of shear demands in particular storeys, a smooth variation of the storey stiffness over the height of the building is required. To achieve this, the vertical stiffness criteria of the National Building of Canada 2015 [22] is observed; the lateral stiffness at any storey is no less than 70 % of any adjacent storey or 80 % of the average stiffness of the three storeys above or below.

3.5. Design of the protected members of the FIEB to withstand elastically the probable forces imposed by the action of the BIEs

To ensure the conditions for the BIEs to fully develop their intended axial force vs. deformation hysteretic response at the design level and beyond, Capacity-Based Design principles are observed. Thus, the non-dissipating members of the FIEBs, i.e. beams, columns, connections and foundations are treated as protected members. As such, they are provided with enough resistance to respond elastically to the forces imposed by the inelastic action of the BIEs. Given that the forces developed by the braces depend on the storey drift level, the probable forces are calculated assuming storey drifts 50 % higher than the design drift in anticipation of ground motions more intense than those associated with the design level. To consider the probable difference between nominal and real material properties, the brace forces are further augmented by the R_y factor corresponding to the brace member's expected material strength. In the case of ASTM A1085 HSS members, $R_y = 1.25$ as per ANSI/AISC 341-16 [23]. As it was shown Section 2.3, since the force-displacement behaviour of BIEs in compression can be approximated with an elastic-perfectly plastic model, there is no need to distinguish between buckling and post-buckling cases when analysing the forces imposed by the BIEs on the rest of the structure, as is the case for CCBs.

3.6. Assessment of the performance of the resulting design

To verify that the performance objectives are fulfilled, the seismic performance of the resulting building should be assessed employing a detailed analysis such as NLRHA. Also, the designer should verify that the structure satisfies service level states and all other relevant ultimate limit states, such as those including wind loading.

4. SEISMIC PERFORMANCE OF MULTI-STOREY FIEBs

To study the seismic performance of FIEBs and to verify the validity of the design procedure, 4-, 8-, and 12-storey prototype buildings based on the plan configuration shown in Fig. 13 (a) were designed for target maximum drift ratios, θ_d , of 2.5 % and 1.5 %. The buildings were also designed as Special Concentrically Braced Frames (SCBFs) following ANSI/AISC 341-16 for the purpose of comparison with traditional braced frame systems. A braced frame configuration with pairs of single diagonals acting in opposite directions in contiguous bays, as shown in Fig. 13 (b) was selected. The braced frame designed and analysed corresponds to one of those situated along the longest dimension of the building. The columns' orientation was chosen so that in-plane deformations of the frame produced bending about their weak axis. The foundation restraints were considered as pins.

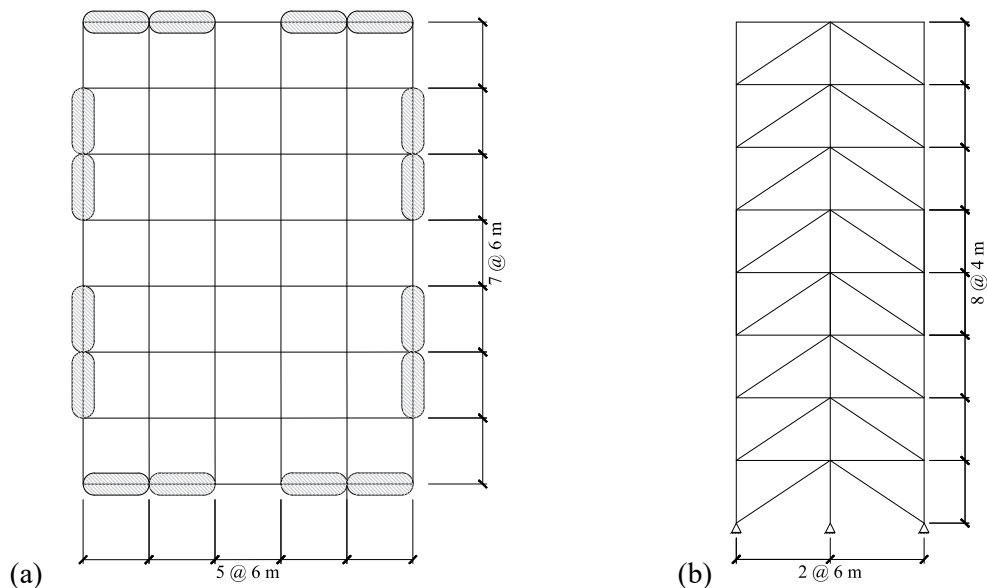


Fig. 13. Plan configuration of considered prototype building (a), with highlighted regions indicating braced bents and vertical configuration of considered SFRS (b) (8-storey frame shown)

4.1. General design criteria

The buildings were located in downtown Los Angeles, CA, (34°05'N, 118°26'W) on a site class C. The general and seismic design criteria and requirements are those from ASCE/SEI 7-16 and the resulting seismic design category is D. The design of the FIEBs was performed following the procedure described above, while for the design of the SCBFs the Equivalent Lateral Force Procedure was employed, with a Response Modification Coefficient, R , of 6. The design seismic ground motion values were taken from the SEAOC/OSHPD Seismic Design Maps online tool (www.seismicmaps.org). The resulting Maximum Considered Earthquake (MCE_R) and Design-Level Earthquake (DE) acceleration response spectra along with their associated non-reduced displacement response spectra, obtained with Eq. (9), are presented in Fig. 14. In consistency with the seismic design criteria of ASCE/SEI 7-16 (2017), the buildings were designed for the demands corresponding to the Design-Level Earthquake. To account for accidental eccentricity, a 10 % increment to the acceleration spectra was applied based on the plan configuration of the building. The dead and live loads considered in the design, as well as the storey seismic masses, are given in Table 2. It was also assumed that the floor slabs present a 0.25 m overhang along the perimeter of the building and that the weight of the exterior wall was 1.5 kPa. Only dead, live and seismic loads were considered, wind loads were not included in this study. For the design of the beams and columns, the requirements for SCBFs from ANSI/AISC 341-16 were observed both for FIEBs and for SCBFs. It was defined that for all buildings the column section would change every three storeys (two in the case of the 4 storey buildings or the topmost storeys of the 8 storey buildings), while the lightest complying beam would be selected at each storey. Formal design of connections, optimization of sections regarding constructability, and assessment of the performance of the buildings under service-level earthquake loads were left out of the scope of the paper.

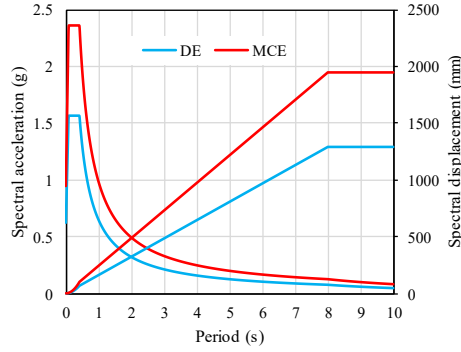


Fig. 14. Acceleration and displacement design response spectra for the prototype buildings

Table 2. Design loads and seismic masses for prototype buildings

Storey	Dead load (kPa)	Live load (kPa)	Seismic mass (kN)
Roof	1.4	0.9	2188
All other storeys	4.1	2.4	6191

4.2. Bracing member design considerations

Given that, as explained previously, the BIE force-deformation models used in design need to correspond to the actual dimensions of the bracing member, it was defined that the total length of the bracing members would be 75 % of the frame diagonal's length (i.e. 5408 mm). This dimension was selected and fixed at the beginning of the design process because the resulting free space was deemed sufficient to accommodate the final dimensions of the columns, beams, and connections that would result from the process. The connections to the frames consist of bolted gusset- and knife-plate arrangements designed to produce in-plane bending of the brace. The introduction of the eccentricity is achieved by means of two side-plates that link the HSS to the knife plate. The pin-like behaviour is assured by including a clearance of twice the knife-plate's thickness between the end of the *eccentering* assembly and its connection to the gusset plate. This configuration was adopted on account of its simplicity and to prevent the storey drifts from imposing in-plane bending moments on the BIEs other than those arising from the eccentricity, thus favouring a simpler and more predictable force-deformation hysteretic behaviour. It was also defined that both the length of the *eccentering* assemblies, L_{ea} , (i.e. the side plates) and the width of the knife-plates would be roughly twice the HSS height, rounded to the closest higher multiple of 5 mm. These dimensions were selected considering that L_{ea} should be such to allow the probable tensile force and moment

produced at the bracing member's end to be transmitted through reasonably sized welds, first to the side plates and then to the knife-plate, and that the width of the knife plate should be such that a reasonable plate thickness would result in order to grant a tension capacity at least equal to the probable tensile force, while having relatively low flexural stiffness. An example of the considered connection and *eccentering* assembly is shown in Fig. 15. The behaviour and performance of the proposed arrangement, including whether the HSS can withstand the cyclic rotational demands it is subjected to, is to be investigated in a later stage of the research program and remains out of the scope of the present paper. In the case of CCBs, an analogous solution was considered but with the knife-plate slotted into the bracing member.

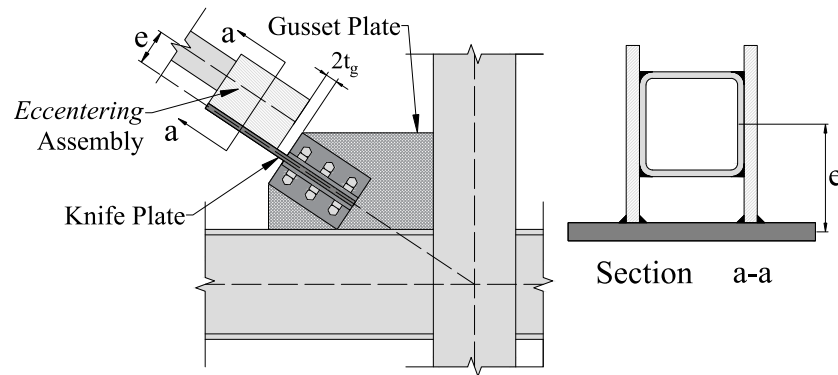


Fig. 15. Example of considered BIE to frame joint connection and *eccentering* assembly

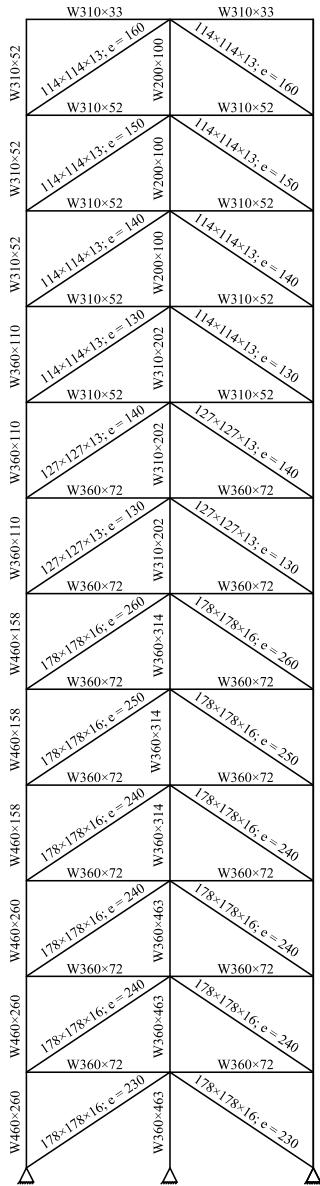
To make the section-eccentricity pair selection process described in Step 4 of the design procedure more efficient, a database containing the relevant design parameters for BIEs made from a wide array of commercially available HSSs was created. The database was prepared using OpenSees models based on the material's nominal mechanical properties (i.e. $F_y = 345$ MPa) and considering eccentricities ranging from null to three times the section height in 10 mm increments and the brace/*eccentering* assembly dimensions described above.

4.3. Resulting design

The resulting bracing members, beams and columns for all buildings are presented in Fig. 16 through Fig. 18. It can be noted for the FIEBs that the proposed design procedure, together with the intention of using the lightest allowable sections, favoured that instead of recurring to frequent

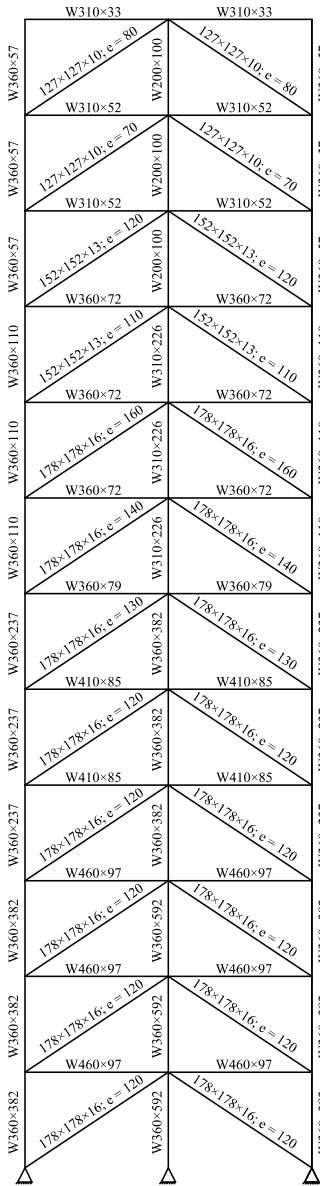
section changes along the building height for the bracing members, a gradually increasing eccentricity for a constant section would be preferred. In addition, the design procedure necessitated that identical section-eccentricity pairs be selected for several adjacent storeys to comply with all the proposed stiffness requirements, indicating that possibly it would have been beneficial to consider a smaller eccentricity increment, such as 5 mm, when preparing the design properties database. However, it is questionable whether such a small resolution in the specified eccentricity would be practical in a realistic fabrication context, considering workmanship and section production tolerances. It can be noted as well that the observed e_0 ratios do not present a wide variation with building height for a given drift ratio. In the buildings with $\theta_d=2.5\%$, the average e/H value varies between 1.07 and 1.28 while in the buildings with $\theta_d=1.5\%$, the observed values are between 0.71 and 0.99. As commented in Section 2.3, for these eccentricity ratios it is expected that the storey shear-deformation stiffness of the BIE pairs will be continuously positive.

The approximate steel tonnage is given in Table 3, broken down by beams and columns and bracing member. For all three building heights, the FIEBs with $\theta_d=2.5\%$ present a lower tonnage than the equivalent SCBF, with the difference increasing with the building height. Although the net weight of the bracing members is slightly higher, the reduction in the protected members given the lower capacity-based design forces compensates and produces an overall lower weight. If design of the foundations had also been included, the difference between the two systems would be even greater. The FIEBs with $\theta_d=1.5\%$, however, were heavier than the SCBFs, with the difference becoming more significant at lower heights.



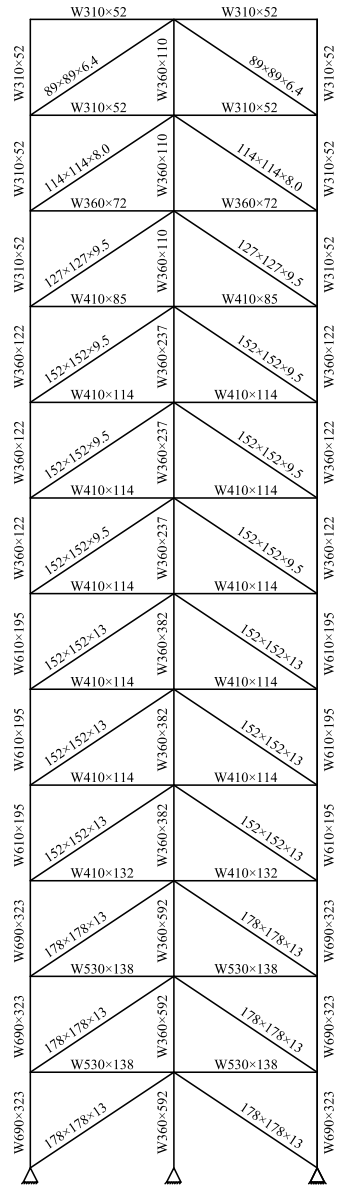
12 Storey FIEB,

$\theta_d = 2.5 \%$,
 $\xi_{eq} = 18 \%$



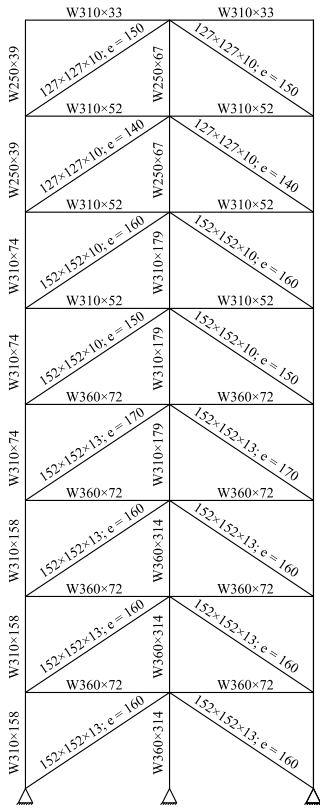
12 Storey FIEB,

$\theta_d = 1.5 \%$,
 $\xi_{eq} = 16 \%$



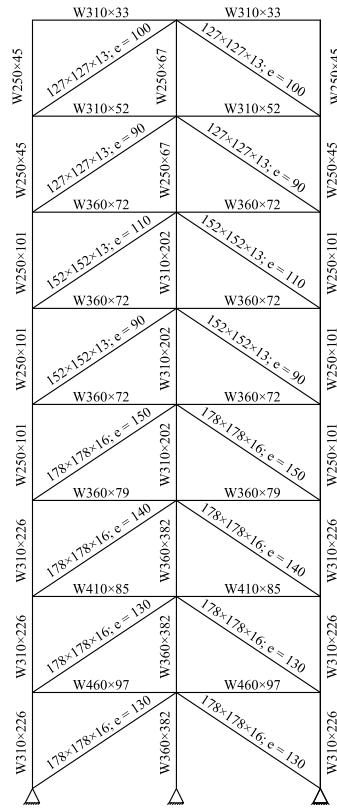
12 Storey SCBF

Fig. 16. Resulting design for 12 storey buildings



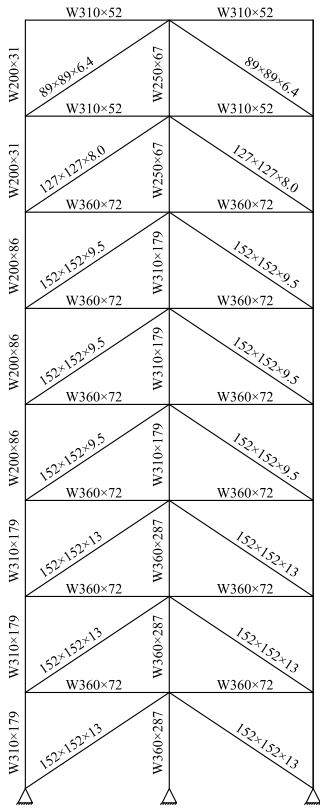
8 Storey FIEB,

$\theta_d = 2.5 \%$,
 $\xi_{eq} = 17 \%$



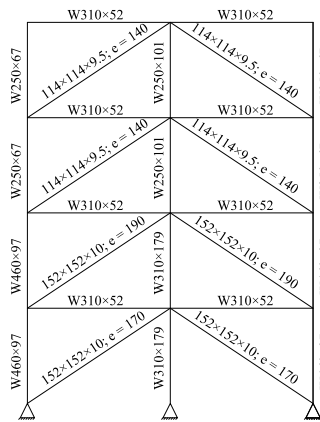
8 Storey FIEB,

$\theta_d = 1.5 \%$,
 $\xi_{eq} = 17 \%$



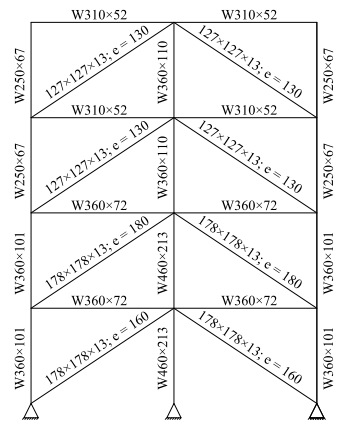
8 Storey SCBF

Fig. 17. Resulting design for 8 storey buildings



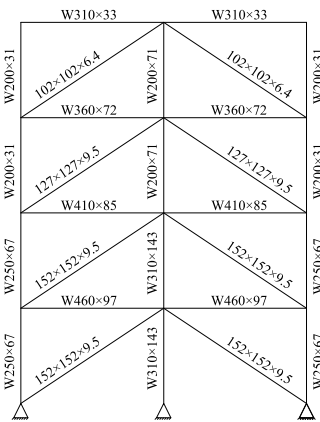
4 Storey FIEB,

$\theta_d = 2.5 \%$,
 $\xi_{eq} = 16 \%$



4 Storey FIEB,

$\theta_d = 1.5 \%$,
 $\xi_{eq} = 17 \%$



4 Storey SCBF

Fig. 18. Resulting design for 4 storey buildings

Table 3. Steel tonnage per braced frame for the resulting designs

Building type	Beams and columns (t)	Bracing members (t)	Total weight (t)
12 Storey SCBF	47.33	7.76	55.09
12 Storey FIEB - $\theta_d=2.5\%$	35.81	9.92	45.73
12 Storey FIEB - $\theta_d=1.5\%$	45.18	11.20	56.38
8 Storey SCBF	19.42	4.67	24.09
8 Storey FIEB - $\theta_d=2.5\%$	18.37	5.16	23.53
8 Storey FIEB - $\theta_d=1.5\%$	22.86	7.1	29.96
4 Storey SCBF	5.08	1.92	7.01
4 Storey FIEB - $\theta_d=2.5\%$	4.93	2.03	6.96
4 Storey FIEB - $\theta_d=1.5\%$	5.61	3.03	8.64

The fundamental and target periods of the structures are shown in Table 4, along with the equivalent damping ratios that were used in the design, as per Step 2 of the design procedure. As expected, the FIEBs are significantly softer structures than the CBFs, especially those designed for the higher target drift ratio, and therefore the anticipated force and acceleration demands are lower. The design equivalent damping ratios showed little variation, ranging between 16 % and 18 % for all 6 FIEBs designed, and not showing any particular trend regarding the building's height or design drift ratio.

Table 4. Fundamental and target periods and design damping ratios for the resulting designs

Building type	Fundamental period (s)	Target period (s)	Design ξ_{eq} (%)
12 Storey SCBF	1.55	-	-
12 Storey FIEB - $\theta_d=2.5\%$	2.59	5.48	18
12 Storey FIEB - $\theta_d=1.5\%$	1.75	3.14	16
8 Storey SCBF	0.93	-	-
8 Storey FIEB - $\theta_d=2.5\%$	1.55	3.61	17
8 Storey FIEB - $\theta_d=1.5\%$	1.15	2.16	17
4 Storey SCBF	0.49	-	-
4 Storey FIEB - $\theta_d=2.5\%$	0.94	2.15	16
4 Storey FIEB - $\theta_d=1.5\%$	0.72	1.32	17

Table 5 presents the rotation demands on the HSSs where they meet the *eccentering* assembly at 1.5 times the target displacement for the 12 storey FIEB with $\theta_d=2.5\%$. The values resulting from the design of this building range from 0.27 rad to 0.43 rad and are similar to those obtained for the other 5 FIEBs. Although not included in the scope of the preliminary study presented in this paper, it is planned to address in a subsequent stage of the research program whether the connections and the HSSs themselves are capable of sustaining such levels of rotation under combined tension force and bending.

Table 5. Rotation demand at the HSS and *eccentering* assembly interface at 1.5 times the target displacement for the 12 storey FIEB with $\theta_d=2.5\%$

Storey	BIE	Rotation demand at 1.5 times the target displacement (rad)
12	114×114×13 – e = 160 mm	0.27
11	114×114×13 – e = 150 mm	0.31
10	114×114×13 – e = 140 mm	0.34
9	114×114×13 – e = 130 mm	0.39
8	127×127×13 – e = 140 mm	0.38
7	127×127×13 – e = 130 mm	0.43
6	178×178×16 – e = 260 mm	0.26
5	178×178×16 – e = 250 mm	0.29
4	178×178×16 – e = 240 mm	0.31
3	178×178×16 – e = 240 mm	0.33
2	178×178×16 – e = 240 mm	0.34
1	178×178×16 – e = 230 mm	0.37

4.4. Non-Linear Response-History Analysis

The NLRHA method was used to assess the performance of the 9 designed frames subjected to seismic demands, both at the DE and at the MCE_R levels, to verify whether the proposed design procedure effectively allows control of the peak storey drifts at the design level and to obtain information about the structural system's response at the maximum considered earthquake level.

- Selection and scaling of ground motion records

For the analyses, 21 out the 22 records that compose the Far-Field Record Set proposed in FEMA P695 [24] were selected. The record of the Cape Mendocino earthquake at Rio Dell Overpass (record sequence number 829) was not included as it is no longer available in the PEER-NGA West2 database [25], from where all records were obtained. Thus, the employed set comprised 42 individual horizontal components obtained from 13 crustal events with magnitudes ranging from 6.5 to 7.6, including 7 that occurred in California, recorded on class C or D sites at an average distance of 16.4 km from the source. The initial scaling of the records was performed using the online tool of the PEER-NGA West2 database, based on the maximum-direction (RotD100) response spectra, using the DBE spectrum as target. A second, common, scaling factor was then applied to all ground motions so that the mean suite spectrum was equal or larger than 90 % of the target spectrum at all periods over the period range of interest. For the MCE_R analyses, a subsequent scaling factor of 1.5 was applied to all records. For scaling purposes, a period range of interest for each building height was selected, with the lower bound corresponding to 0.2 times the shortest

fundamental period of the group of structures (e.g. 0.1 s for the 4-storey SCBF) and the higher bound corresponding to the target period of the most flexible structure in the group (i.e. the FIEB with $\theta_d = 2.5\%$). Instead of specific period ranges of interest for each particular building, the use of a common period range for each group with equal number of storeys was preferred as it enables the direct comparison of the buildings' response to identical seismic demands. Thus, the period ranges of interest were from 0.31 s to 5.48 s for the 12-storey buildings, from 0.19 s to 3.61 s for the 8-storey buildings, and from 0.1 s to 2.15 s for the 4-storey buildings. Figure 19 presents the spectra of the scaled employed ground motion suite, the period ranges of interest and the target DE spectrum.

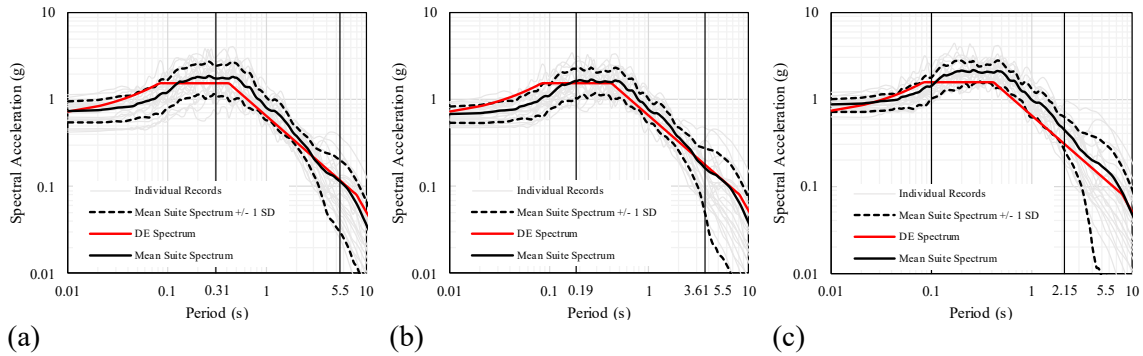


Fig. 19. Mean Spectra of the employed scaled ground motion suite, period ranges of interest, and target DE spectrum: (a) 12-storey buildings %; (b) 8-storey buildings; (c) 4-storey buildings

4.4.1. Modelling considerations

Plane models of the designed frames were created using fiber-based elements in OpenSees. Probable material resistances were considered: $R_y F_y = 431$ MPa for the HSSs and $R_y F_y = 380$ MPa for the beams, columns and plates. An initial out-of-straightness of a thousandth of the element length was applied to all frame elements; which corresponds to the fabrication tolerance in North American codes [14, 15]. For the braces, the imperfection was introduced such that it increased the effective eccentricity, thus reducing their stiffness and strength. The gravitational loads applied were 100 % of the dead loads plus 50 % of the live loads as per Clause 16.3.2 of ASCE/SEI 7-16. The knife-plates and *eccentering* assemblies were explicitly modelled, while the rest of the connections to the frame joints were modelled as rigid links. At each storey, the mass was

introduced lumped in the central node, and diaphragm constraints were applied. Rayleigh damping of 2.5 % was considered for the structures, and P- Δ effects were included in the models using the leaning column approach. In the analyses, an additional factor of 1.1 was applied to the ground motion records to ensure consistency between demand and capacity as braced frame strength was increased by 10 % to account for accidental torsion effects in design. Numerical tests were performed to verify that the residual stresses and in-section variation of F_y across the HSSs produced no significant influence on the response of the FIEBs; these effects were therefore not included in the final analyses.

4.4.2. Results and discussion

To determine whether the proposed design procedure allows one to effectively anticipate the storey drift ratios that the buildings will develop under seismic action at the design earthquake level, the mean values of the peak storey drifts under the DE level ground motions are plotted for all 6 FIEBs, as shown in Fig. 20. For each structure, the mean of the peak values, and the differences with respect to the target are reported in Table 6. For the 12- and 8-storey FIEBs designed for $\theta_d = 2.5$ %, the mean peak storey drifts in the table are lower than the design limit, which can be considered satisfactory, although the difference, in particular for the 12-storey building, can be in part interpreted as a consequence of the design procedure not considering the effects of higher modes of vibration in the selection of the target displaced shape. In the case of the 4-storey building with $\theta_d = 2.5$ %, however, the difference of 25.6 % indicates that the design procedure did not control the drift as intended. As for the buildings designed for $\theta_d = 1.5$ %, the 12- and 8- storey buildings present mean peak storey drift values remarkably close to the design target, while the 4-storey FIEB developed peak storey drifts on average 66.7 % larger than the target level. The higher than anticipated storey drifts concerning the 4-storey buildings can be explained by the mean suite response spectrum being on average 40 % higher than the design spectrum between 0.1 s and 2.15 s, as can be observed in Fig. 19 (c). This is a consequence of the requirement for the mean suite

response spectrum not to be inferior by more than 10 % to the target spectrum over the period range of interest.

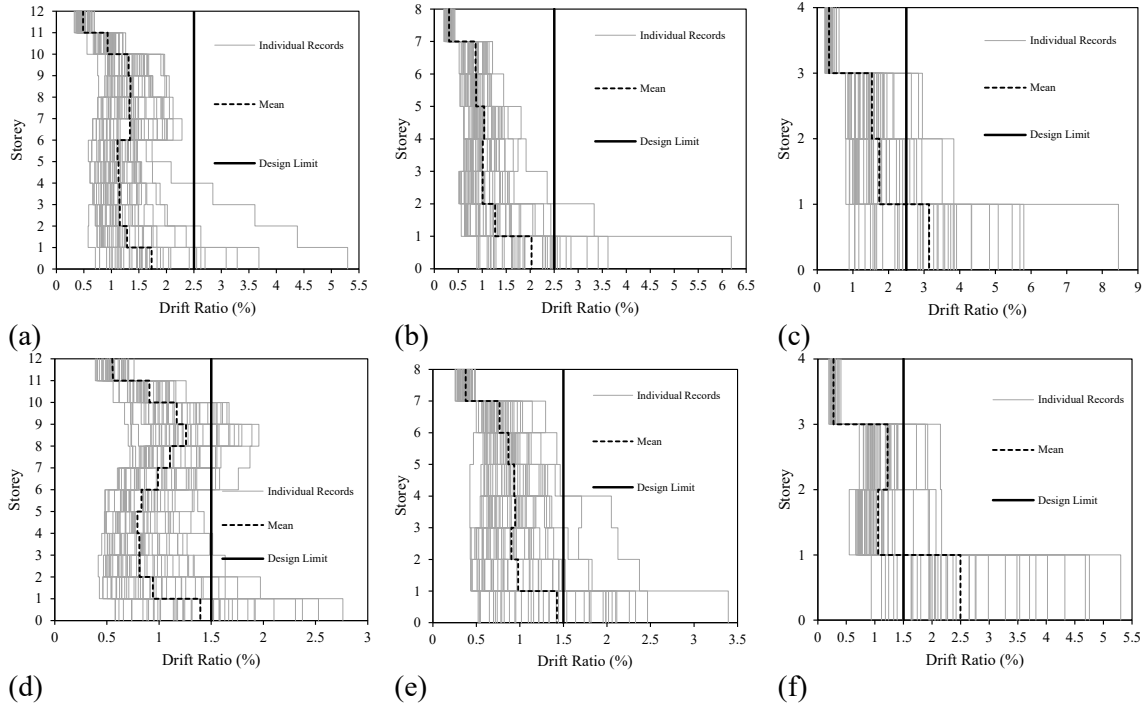


Fig. 20. Peak storey drifts at DE level for FIEBs: (a) 12-storey with $\theta_d = 2.5\%$; (b) 8-storey with $\theta_d = 2.5\%$; (c) 4-storey with $\theta_d = 2.5\%$; (d) 12-storey with $\theta_d = 1.5\%$; (e) 8-storey with $\theta_d = 1.5\%$; (f) 4-storey with $\theta_d = 1.5\%$

Table 6. Mean peak storey drifts at DE level compared with design targets

Building type	Mean Peak Storey Drift (%)	Difference (%)
12 Storey FIEB - $\theta_d = 2.5\%$	1.73	-30.7
8 Storey FIEB - $\theta_d = 2.5\%$	2.02	-19.2
4 Storey FIEB - $\theta_d = 2.5\%$	3.14	25.6
12 Storey FIEB - $\theta_d = 1.5\%$	1.40	-6.67
8 Storey FIEB - $\theta_d = 1.5\%$	1.43	-4.67
4 Storey FIEB - $\theta_d = 1.5\%$	2.50	66.7

The effectiveness of the capacity-based protection measures included in the proposed design procedure is evaluated by comparing the peak storey shears that developed in the FIEBs under the MCE_R level ground motions with those used to design the protected FIEB elements, i.e. storey shears determined at 1.5 times the storey drifts expected at the DE level, as presented in Fig. 21. For all FIEBs but one, the mean of the peak storey shears is lower than the capacity-based design shear used to dimension the beams and columns. In the case of the 4-Storey FIEB designed for $\theta_d = 1.5\%$, the mean peak storey shears are in practical terms equal to the design forces, being higher by less than 1.0 %. This indicates that the drift-based amplification contained in the design

procedure could adequately reduce the probability of excessive demand on the protected elements at the MCE_R level, and thus of the occurrence of an unwanted failure mechanism. However, for all buildings there were ground motion records for which the capacity-based design storey shear was exceeded; which is attributed to the fact that the peak drifts surpassed the assumed 1.5 times the design level in several cases, which is not surprising given the number and variability of the records considered. To effectively annul the possibility for a ground motion to produce storey shears larger than the design storey shear, it would be necessary either to calculate the design storey shears based on the ultimate tension force that can be developed by the bracing members (i.e. $R_y F_y A_g$), or to implement a fuse-like device in the brace connections that would pose a cap to the maximum forces transmitted to the protected elements. As the first option would eliminate one of the purported benefits of FIEBs over CBFs, to reduce the costs by limiting the design forces on the protected elements, the second option could represent a reasonable alternative to be investigated in a subsequent stage of the research program.

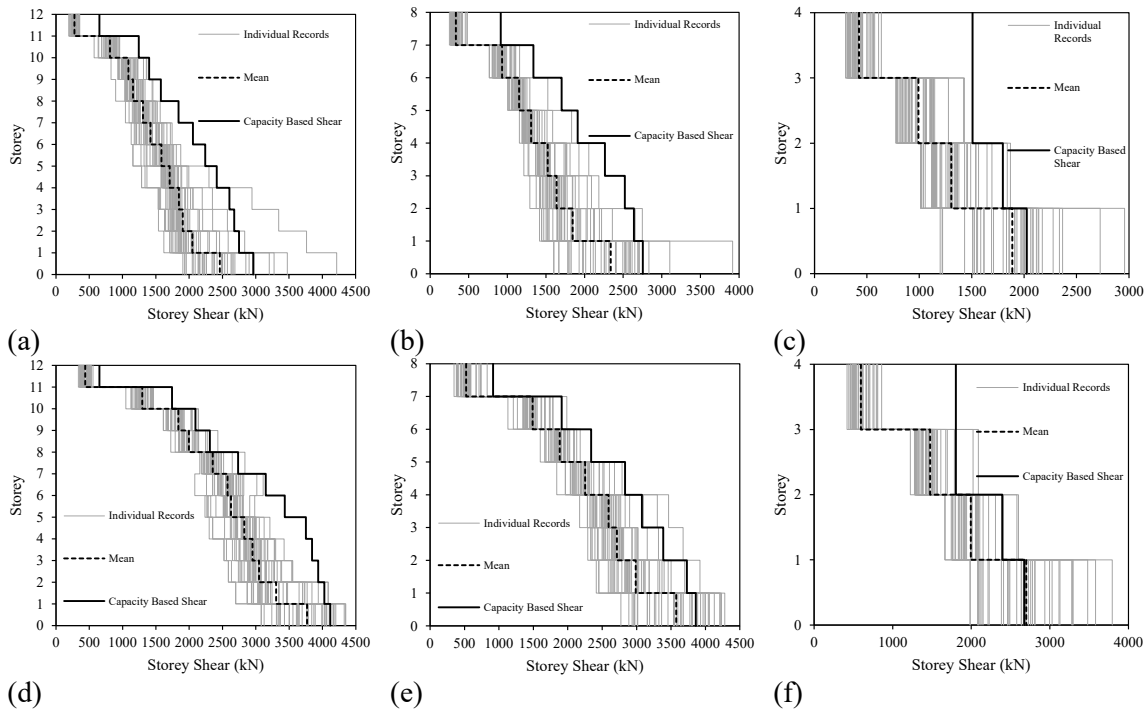
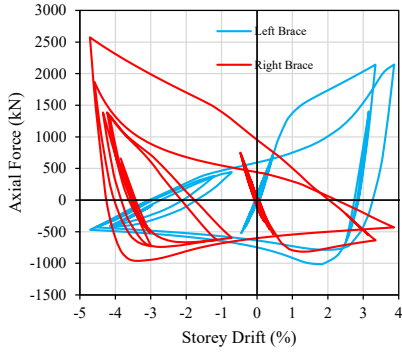


Fig. 21. Maximum storey shears at MCE_R level for FIEBs: (a) 12-storey with $\theta_d = 2.5\%$; (b) 8-storey with $\theta_d = 2.5\%$; (c) 4-storey with $\theta_d = 2.5\%$; (d) 12-storey with $\theta_d = 1.5\%$; (e) 8-storey with $\theta_d = 1.5\%$; (f) 4-storey with $\theta_d = 1.5\%$

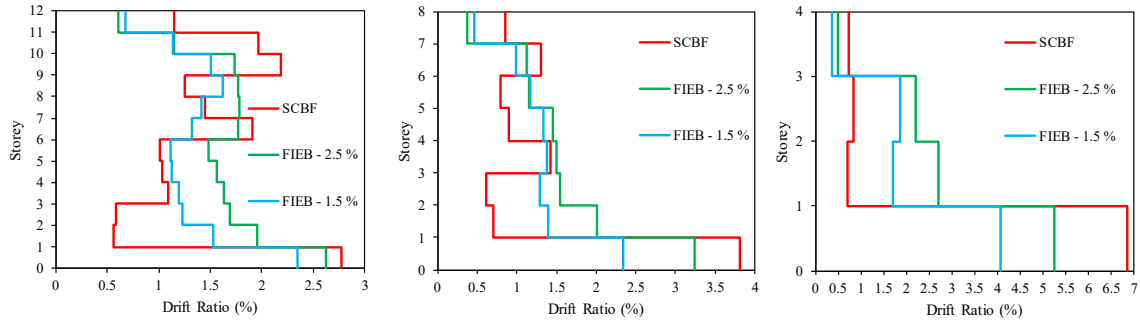
The number of ground motions at the MCE_R level causing unacceptable storey drifts for each structure is reported in Table 7. In this study, storey drifts of 5 % and 30 % were arbitrarily set as the thresholds for unacceptable response and structural collapse, respectively. No collapses were observed in the frames studied according to this criterion. As shown, the SCBFs presented worse overall performance at the MCE_R level than the FIEBs, in terms of unacceptable responses. Finite element analysis of the BIEs at the first storey was performed to verify that these braces could sustain the seismic drift demand without developing local buckling. In the FE analyses, shell-element models of the BIEs in Abaqus were subjected to the displacement histories recorded from the OpenSees analyses that produced maximum drifts close to 5 %. In Fig. 22, an example of the resulting axial force vs. storey drifts plots resulting from these analyses is shown, along with the deformed shape of the BIE model at the point of maximum compression. The analyses showed that the BIEs could withstand that drift level without developing local buckling, indicating that the unacceptable response threshold could be larger than 5 % storey drifts in terms of brace inelastic response. The mean peak and residual storey drifts under the MCE_R level ground motions for the SCBFs and FIEBs are compared in Figs. 23 and 24, respectively. As expected, storey drifts for the FIEBs designed with 1.5 % target drift are consistently lower than those sustained by the FIEBs designed using a target drift of 2.5 %. Compared to the FIEBs, the SCBFs exhibited markedly larger peak and residual drifts at the first storey at the MCE_R level. Conversely, the FIEBs presented larger drifts for most other storeys, showing that the system can produce a more even distribution of the drift demand over the building height. Although not shown here, similar differences were observed at the DE level; the SCBFs experienced mean peak storey drifts smaller than both FIEBs for the 12-storey buildings, and larger than the FIEBs with $\theta_d = 1.5$ % for the 8- and 4-storey buildings.

Table 7. Number of unacceptable responses for MCE_R NLRHA

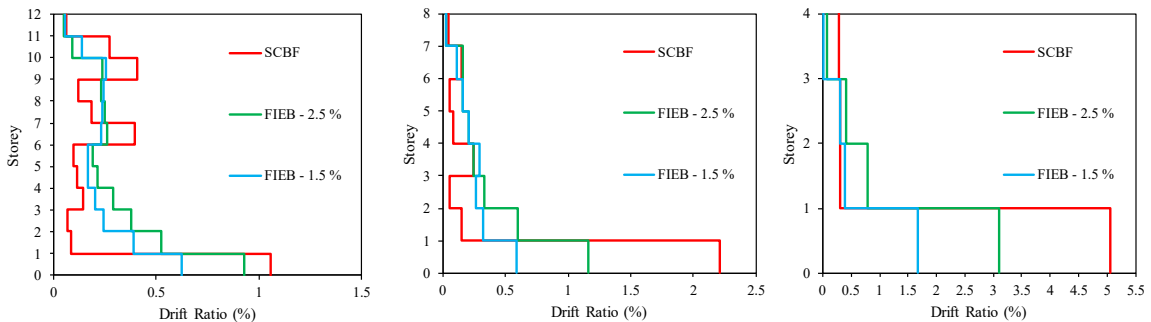
Building type	Unacceptable results ($\theta_{max} > 5\%$)
12 Storey SCBF	3
12 Storey FIEB - $\theta_d = 2.5\%$	1
12 Storey FIEB - $\theta_d = 1.5\%$	2
8 Storey SCBF	11
8 Storey FIEB - $\theta_d = 2.5\%$	2
8 Storey FIEB - $\theta_d = 1.5\%$	0
4 Storey SCBF	22
4 Storey FIEB - $\theta_d = 2.5\%$	18
4 Storey FIEB - $\theta_d = 1.5\%$	10



(a) (b)
 Fig. 22. Response of first storey braces of the 12-storey FIEB with $\theta_d = 2.5\%$ for a ground motion that produced maximum drift close to 5%: (a) axial force vs. storey drift; (b) deformed shape at maximum drift for right brace finite element model



(a) (b) (c)
 Fig. 23. Comparison of mean peak storey drifts at MCE_R level: (a) 12-storey buildings; (b) 8-storey buildings; (c) 4-storey buildings



(a) (b) (c)
 Fig. 24. Comparison of mean residual storey drifts at MCE_R level: (a) 12-storey buildings; (b) 8-storey buildings; (c) 4-storey buildings

The difference in the observed peak and residual drifts in SCBFs and FIEBs can be explained by the essentially distinct post-yielding stiffness that each system possesses. While the conventional concentrically braced frame boasts a nearly null stiffness after yielding of the tension brace, thus opposing no resistance to further displacement demand, the frame with intentionally eccentric braces benefits from a significant post-yielding stiffness that is not reduced until very large deformations, counterbalancing large displacement pulses. This is evident from the comparison of the first storey shear vs. drift history plots of SCBFs and FIEBs for some of the ground motions, which produced unacceptable response from the SCBFs, while the FIEBs performed remarkably well. One of such examples is presented in Fig. 25, for the ground motion record with sequence number 721 in PEER NGA West 2 database, 90° component, and scale factor of 2.59 for MCE_R including 10 % increase for accidental torsion.

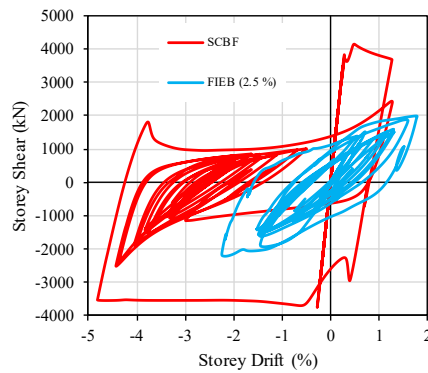


Fig. 25. First storey shear vs. drift history plot for 12-storey SCBF and FIEB with $\theta_d = 2.5\%$ for ground motion number 721, 90° component at MCE_R level

5. CONCLUSIONS

It was shown that the characteristics of BIEs potentially enable this recently proposed type of brace to overcome some of the most prominent drawbacks of traditional CCBs; notably, those associated with their high inherent stiffness, their susceptibility to local buckling and subsequent low-cycle fatigue-induced fracture, and their tendency to concentrate drift demands in a limited number of storeys. A seismic design procedure based on the Direct Displacement Based Design approach was proposed in an effort to explicitly account for the particular force-displacement response of BIEs.

The proposed procedure was employed in the design of hypothetical buildings located in a high seismic hazard region. The performance of the resulting structures was assessed through Non-Linear Response-History Analysis, using an established ground motion record suite. It was verified, albeit preliminarily, that the proposed design procedure could be considered adequate for the design of Frames with Intentionally Eccentric Braces as it produces buildings that, on average, comply with the selected target maximum drifts and performance objectives. Although the maximum storey drifts were larger than the design targets for the FIEBs with shorter periods, the results can be regarded as auspicious, considering that the scaled ground motion record suite used in the analysis produced demands larger than those anticipated in the design. Moreover, the forces in the capacity-protected elements did not surpass, on average, the threshold considered in design. Furthermore, the results obtained showed that FIEBs may present a safer response to severe ground motions than SCBFs, because the maximum and residual storey drifts were significantly lower, owing to the substantial secondary stiffness of BIEs. Also, it was shown that FIEBs designed for relatively high target drift ratios can result in economic advantages over SCBFs.

Further studies, however, are required to refine the equivalent damping ratios and design displacement vectors used in the design procedure, and to address an effective way of controlling or capping the maximum storey shears in anticipation of ground motions more severe than expected. Research is also necessary to evaluate the performance of the proposed *eccentering* assembly and connections, and to validate or refute the preliminary fracture life equation herein proposed.

ACKNOWLEDGMENTS

The first author wishes to thank Universidad de Costa Rica for financing the undertaking of his doctoral studies. The authors would also like to acknowledge DPHV Structural Consultants and ADF Group Inc. for their generous technical and financial support, as well as the Natural Sciences and Engineering Research Council of Canada (NSERC), the Fonds de Recherche du Québec –

Nature et Technologies (FRQ-NT) and the Centre d'Études Interuniversitaire des Structures sous Charges Extrêmes (CEISCE).

REFERENCES

- [1] Tang, X., & Goel, S. (1989). Brace fractures and analysis of phase I structure. *ASCE Journal of Structural Engineering*, 115(8): 1960-1976.
- [2] Tremblay, R. (2002). Inelastic seismic response of steel bracing members. *Journal of Constructional Steel Research*, 58(5-8) 665-701.
- [3] Constanzo, S., D'Aniello, M., Landolfo, R. (2019). Proposal of design rules for ductile X-CBFS in the framework of EUROCODE 8. *Earthquake Engng Struct Dyn.*, 48:124-151
- [4] Skalomenos, K., Inamasu, H., Shimada, H., & Nakashima, M. (2017). Development of a Steel Brace with Intentional Eccentricity and Experimental Validation. *ASCE Journal of Structural Engineering*. DOI: 10.1061/(ASCE)ST.1943-541X.0001809.
- [5] ASCE. (2017). *Minimum Design Loads for Buildings and Other Structures*, ASCE/SEI 7-16. Reston, VA.: American Society of Civil Engineers.
- [6] McKenna, F. (1997). *Object Oriented Finite Element Programming: Framework for Analysis, Algorithms and Parallel Computing* Ph.D. Dissertation, University of California, Berkeley.
- [7] Agüero, A., Izvernari, C., & Tremblay, R. (2006). Modelling of the Seismic Response of Concentrically Braced Steel Frames using the OpenSees Analysis Environment. *International Journal of Advanced Steel Construction*, 242-274.
- [8] Uriz, P., Filippou, F., & Mahin, S. (2008). Model for Cyclic Inelastic Buckling of Steel Braces. *ASCE Journal of Structural Engineering*, 619-628.
- [9] Dassault Systèmes. (2018). *Abaqus/CAE 2019*. Dassault Systèmes Simulia Corp. Providence, RI.
- [10] Fell, B., Kanvinde, A., & Deierlein, G. (2010). *Large-Scale Testing and Simulation of Earthquake Induced Ultra Low Cycle Fatigue in Bracing Members Subjected to Cyclic Inelastic Buckling*. Stanford: John A. Blume Earthquake Engineering Center.
- [11] Koval, I. (2018). *Accounting for Cold Working and Residual Stress Effects on the Axial Strength of HSS Bracing Members*, Masters thesis, Polytechnique Montréal. Montréal.
- [12] Tremblay, R., Archambault, M.H., & Filiatrault, A. (2003). Seismic response of concentrically braced steel frames made with rectangular hollow bracing members. *Journal of Structural Engineering (ASCE)*. 129(12): 1626-1636
- [13] Chopra, A. (2012). *Dynamics of Structures*, fourth edition. Berkeley: Pearson.
- [14] AISC. (2016). *Specification for Structural Steel Buildings*, ANSI/AISC 360-16. Chicago, IL.: American Institute for Steel Construction.

- [15] CSA. (2014). CSA S16-14: Design of steel structures. Toronto, ON: Canadian Standards Association (CSA).
- [16] Priestley, M., Calvi, G., & Kowalsky, M. (2007). Displacement-Based Seismic Design of Structures. Pavia: IUSS Press.
- [17] Wijesundara, K., Rajeev, P. (2012). Direct Displacement-Based Design of steel concentric braced frames structures. Australian Journal of Structural Engineering, 13 (3), 243-257.
- [18] O'Reilly, G. Goggins, J., Mahin, S. (2012). Performance-based design of a self-centering concentrically braced frame using the Direct Displacement-Based Design Procedure. Proc. 15th World Conference on Earthquake Engineering, Lisbon, Portugal, Paper no. 918
- [19] Al-Mashaykhi, M., Rajeev, P., Wijesundara, K., & Hashemi, M. (2019). Displacement profile for displacement based seismic design of concentric braced frames. Journal of Constructional Steel Research, 233-248.
- [20] Wijesundara, K., Nascimbene, R., & Sullivan, T. (2011). Equivalent viscous damping for steel concentrically braced frame structures. Bull Earthquake Eng, 9:1535-1558.
- [21] European Committee for Standardization – CEN (2004). EN 1998-1:2004 Eurocode 8: Design of structures for earthquake resistance – Part 1: General rules, seismic action and rules for buildings. CEN, Brussels, Belgium
- [22] NRCC. (2015). National Building Code of Canada 2015, 14th ed. Ottawa, ON: National Research Council of Canada (NRCC).
- [23] AISC. (2016). Seismic Provisions for Structural Steel Buildings, ANSI/AISC 341-16. Chicago, IL.: American Institute for Steel Construction.
- [24] FEMA. (2009). Quantification of Building Seismic Performance Factors, FEMA P695. Redwood City, CA.: Federal Emergency Management Agency (FEMA).
- [25] PEER (2019). The PEER Ground-Motion Selection Web Application. Pacific Earthquake Engineering Research Center, University of California, Berkeley. <http://ngawest2.berkeley.edu/>